CORA Cork Open Research Archive
Cartlann Taighde Oscailte Chorcaí

Title	The magnetic field strength of the Faraday screen surrounding the radio galaxy Coma A
Authors	Knuettel, Sebastian;O'Sullivan, S. P.;Curiel, S.;Emonts, B. H. C.
Publication date	2018-11-10
Original Citation	Knuettel, S., O'Sullivan, S. P., Curiel, S. and Emonts, B. H. C. (2018) 'The magnetic field strength of the Faraday screen surrounding the radio galaxy Coma A', Monthly Notices of the Royal Astronomical Society, 482(4), pp. 4606-4616. doi: 10.1093/mnras/sty3018
Type of publication	Article (peer-reviewed)
Link to publisher's version	10.1093/mnras/sty3018
Rights	© 2018, the Authors. Published by Oxford University Press on behalf of the Royal Astronomical Society. All rights reserved.
Download date	2026-11-02 19:43:49
Item downloaded from	https://hdl.handle.net/10468/7954



UCC
University College Cork, Ireland
Coláiste na hOllscoile Corcaigh

Monthly Notices
of the
ROYAL ASTRONOMICAL SOCIETY

MNRAS **482,** 4606–4616 (2019)
Advance Access publication 2018 November 10

doi:10.1093/mnras/sty3018

The magnetic field strength of the Faraday screen surrounding the radio galaxy Coma A

S. Knuettel,[1]★ S. P. O'Sullivan,[2] S. Curiel[3] and B. H. C. Emonts[4]

[1]*Department of Physics, University College Cork, Cork, Ireland*
[2]*Hamburger Sternwarte, Universität Hamburg, Gojenbergsweg 112, D-21029 Hamburg, Germany;*
[3]*Instituto de Astronomía, Universidad Nacional Autónoma de México (UNAM), A.P. 70-264, 04510 México, D.F., Mexico*
[4]*National Radio Astronomy Observatory, 520 Edgemont Road, Charlottesville, VA 22903, USA*

Accepted 2018 November 3. Received 2018 October 30; in original form 2018 August 1

ABSTRACT

Studying the interaction between AGN jets and lobes and their surrounding environment is important in order to understand how they transfer energy to their environment as well as determining the intrinsic physical properties of the sources themselves. This paper presents broad-band VLA polarization and Faraday rotation observations of the radio galaxy Coma A (3C 277.3) from 1 to 4 GHz, including archival VLA observations at 4.9 and 15 GHz. Through broad-band polarization model-fitting, we find that an external Faraday screen with a turbulent magnetic field provides an appropriate description to most of the data. By combining the polarization and Faraday rotation results with previous H α observations, we identified the Hα-emitting gas as the Faraday screen responsible for the observed Faraday depolarization. We were able to derive the magnetic field strength in the Hα-emitting gas, finding typical field strengths of $\sim$1 μG, which is consistent with studies of the intragroup medium local to other radio galaxies. However, we find a highly depolarized region of the southern lobe coincident with a Hα filament that has a field strength comparable to the equipartition field strength in the radio lobe (i.e. $\gtrsim$36 μG). This implies that the Hα filament is internal to the radio emitting plasma. Such clear examples of internal Faraday depolarization are rare, thus providing another key insight into the evolution of radio galaxies and their ability to provide significant feedback on the local gas that would otherwise cool and form stars.

Key words: techniques: polarimetric – galaxies: active – galaxies: individual: Coma A – galaxies: magnetic fields – radio continuum: galaxies.

1 INTRODUCTION

The radio-emitting structures in the vicinity of supermassive black holes in the centres of active galaxies display a large variety of morphological properties. It is a long standing debate to what extent the differences between different types of radio sources are due to intrinsic properties of the central engine ('nature') or the properties of the interstellar and intergalactic medium (ISM and IGM) surrounding the central engine and host galaxy ('nurture'). Investigating this 'nature versus nurture' debate for nearby radio galaxies is vital for understanding the properties and evolution of radio galaxies throughout the Universe (e.g. Fabian 2012; Heckman & Best 2014, and references therein).

Here we study one such case, where there are clear interactions between the radio lobes and the surrounding gas, in the nearby radio galaxy Coma A (Bridle et al. 1981; van Breugel et al. 1985; Tadhunter et al. 2000; Morganti et al. 2002; Worrall, Birkinshaw & Young 2016). In particular, we present a study of the combination of wide-band polarimetric radio observations and deep Hα images. This combination provides a powerful tool to investigate the interactions between the lobes and their surrounding environment: the wide-band radio observations allow us to investigate the polarization and magnetic field structure of the radio emitting lobes and how this changes with wavelength, and the Hα measurements allow estimation of the electron density in the shocked gas surrounding the lobes, which in turn enables the calculation of the magnetic field strength in the gas containing the free electrons using the effect of Faraday rotation.

1.1 Coma A

Coma A is a radio galaxy at redshift $z = 0.0857$ (Bridle et al. 1981) corresponding to a comoving radial distance of 371.6 Mpc and angular scale of 1.659 kpc arcsec^{-1} (Wright 2006) using the values of $H_0 = 67.74\,\mathrm{km\,s^{-1}\,Mpc^{-1}}$, $\Omega_M = 0.3089$, and $\Omega_\Lambda = 0.6911$ from

★ E-mail: s.knuettel@mars.ucc.ie

© 2018 The Author(s)
Published by Oxford University Press on behalf of the Royal Astronomical Society

Downloaded from https://academic.oup.com/mnras/article-abstract/482/4/4606/5173058 by University College Cork user on 21 May 2019

the Plank 2015 results (Planck Collaboration XI 2016). The source has two distinct radio lobes and an angular size of 45 arcsec in the north–south direction. Coma A is classified as a Fanaroff–Riley II galaxy in Fanaroff & Riley (1974). The northern lobe shows a bright hotspot, and the southern lobe has a bright plume expanding into a lobe structure. This plume is at a deflected angle to the expected jet direction due to a collision with a gas cloud, decelerating the jet and giving it the features of an FRI structure (van Breugel et al. 1985). Due to this feature and the fact that the power of this radio galaxy is lower that most FRII galaxies, Coma A is on the border between FRI and II classification (Fanaroff & Riley 1974, table 1). It was classified as an FRI for this reason in Chiaberge, Capetti & Celotti (1999). It is an example of a hybrid morphology radio source (HyMoRS; Gopal-Krishna & Wiita 2000a; Gawronski et al. 2006; de Gasperin 2017).

Large-scale arcs and filaments of Hα emission have been observed surrounding the radio lobes (Tadhunter et al. 2000), which closely match the shape of the radio lobes of Coma A. The origin of this ionized gas is discussed in depth in Tadhunter et al. (2000). The most likely cause for the ionization is the shock from the expanding radio lobes moving into a region of neutral gas surrounding the host galaxy. The origin of the gas has been investigated with H I absorption observations of Coma A. These show the presence of H I local to both lobes and suggest that a large-scale gas disc surrounds the galaxy, into which the radio lobes are expanding (Morganti et al. 2002). The origin of the gas itself is most likely from a merger in the Coma A host galaxy. The existence of such gas around the lobes is also observed in the X-ray. In particular, Worrall et al. (2016, figure 7) show how regions of diffuse X-rays in the local environment display an anticorrelation to the Hα filaments. They argue that the original group atmosphere has been shock ionized and now surrounds the lobes, causing the extended X-rays and the Hα filaments.

In this paper, we present new wide-band dual-polarization observations of Coma A using the VLA. We use these and archival VLA observations to investigate how the Hα-emitting gas and radio lobes interact, through an analysis of the Faraday rotation of the polarized radio emission.

1.2 Polarization and Faraday rotation

Radio galaxy lobes emit synchrotron radiation from relativistic electrons accelerated by magnetic fields. The observed flux density typically obeys a power law with frequency, $S \propto \nu^{+\alpha}$, where S is the observed radio flux density, ν is the observing frequency, and α is the spectral index. Synchrotron radiation is intrinsically highly linearly polarized, with a theoretical maximum limit of ∼70 per cent. The linear polarization is measured using the Stokes parameters, Q and U, where the complex linear polarization (P) is defined as

$$P = Q + \mathrm{i}U = p_0 I \mathrm{e}^{2\mathrm{i}\chi}, \tag{1}$$

where p_0 is the intrinsic degree of polarization (i.e at zero wavelength), χ is the observed polarization angle, and I is the total intensity. The fractional polarization, p, and polarization angle, χ, are described as follows:

$$p = \frac{|P|}{I} = \frac{\sqrt{Q^2 + U^2}}{I}, \tag{2}$$

$$\chi = \frac{1}{2} \arctan\left(\frac{U}{Q}\right). \tag{3}$$

The observed polarization angle, χ, changes with wavelength due to Faraday rotation. This effect acts on a polarized electromagnetic wave as it passes through a region with free electrons and magnetic field along the line of sight. The polarization angle changes linearly as a function of wavelength squared in the simplest case,

$$\chi = \chi_0 + \mathrm{RM}\lambda^2, \tag{4}$$

where χ_0 is the intrinsic polarization angle and RM is the Faraday rotation measure. This RM value is calculated as follows (Burn 1966):

$$\mathrm{RM} = 0.81 \int n_\mathrm{e}\,(l)\, B_\parallel \mathrm{d}l, \tag{5}$$

where $B_\parallel$ is the line-of-sight component of the magnetic field in μG, n_e is the electron density in cm^{-3}, and dl is an element along the path along the line of sight in parsecs.

It is commonly observed that the fractional polarization, p, tends to decrease towards longer wavelengths, an effect known as depolarization. One of the most common models associated with this phenomenon is external Faraday dispersion (Sokoloff et al. 1998), where an external screen with free electrons and a turbulent magnetic field depolarizes the signal within the observing beam, due to the different resulting Faraday rotations occurring along individual lines of sight within the beam. It is possible to fit models to observed data with good λ^2 coverage in order to estimate the parameters of the source polarization and turbulent screen (e.g. O'Sullivan et al. 2012). The model used in this paper has a single RM component and an external depolarizing screen, motivated in part by the picture of a shell of ionized gas surrounding the lobes of Coma A

$$p\,(\lambda) = p_0 \mathrm{e}^{2\mathrm{i}(\chi_0 + \mathrm{RM}\lambda^2)} \mathrm{e}^{-2\sigma_\mathrm{RM}^2 \lambda^4}. \tag{6}$$

Here, $p(\lambda)$ is the fractional polarization as a function of wavelength. The first exponential term is the complex linear polarization (equation 1) with the observed polarization angle defined as in equation (4). The second exponential term represents the depolarization by an external Faraday screen, where σ_RM is the standard deviation of the RM within the telescope beam, due to the turbulent magnetic field in the ionized gas. Using equations (1) and (6), the fractional Stokes Q and U parameters, $q(\lambda)$ and $u(\lambda)$, are described as follows:

$$q\,(\lambda) = p_0 \cos\left(2\chi_0 + 2\mathrm{RM}\lambda^2\right) \mathrm{e}^{-2\sigma_\mathrm{RM}^2 \lambda^4}, \tag{7a}$$

$$u\,(\lambda) = p_0 \sin\left(2\chi_0 + 2\mathrm{RM}\lambda^2\right) \mathrm{e}^{-2\sigma_\mathrm{RM}^2 \lambda^4}. \tag{7b}$$

These equations can be fit to observed data by creating cubes of the q and u images from the wide band observations. This fitting yields calculated values of χ_0, RM, σ_RM, and p_0 for each pixel.

2 OBSERVATIONS AND DATA REDUCTION

2.1 Wide band VLA observations

The Karl G. Jansky Very Large Array (VLA) observations in L (994–2006 MHz) and S (1988–4012 MHz) bands were taken on the 2013 December 29 and 2013 September 2013, respectively, in the VLA B configuration. The flux, phase, and bandpass calibrations were done with regular scans of 3C 286, which is close to Coma A, every 20 min. A summary can be seen in Table 1, where ν_1 is the starting frequency of the observing band and ν_2 is the final frequency. The width of each channel in the wideband setup is $\Delta\nu$. The date is the observing date while t is the total integration time on Coma A for that observation.

Downloaded from https://academic.oup.com/mnras/article-abstract/482/4/4606/5173058 by University College Cork user on 21 May 2019

Table 1. Table outlining the VLA observations of Coma A.

Configuration	ν_1 MHz	ν_2 MHz	$\Delta\nu$ MHz	Date	t h
VLA B	1988	4012	2	2013 Sep 27	1.75[a]
VLA B	994	2006	1	2013 Dec 29	1.79

Note. [a]Due to an unknown error in the instrumental polarization calibration, only the final two thirds of these scans had correct polarization calibration applied and were usable for polarization measurements. The Stokes *I* data are unaffected.

Table 2. Table outlining the archival VLA observations of Coma A.

Project	ν MHz	$\Delta\nu$ MHz	Configuration	Date	t h
VANB[a]	4885	50	VLA B	1981 Jun 1	4.1
AB348	14940	100[b]	VLA C	1985 Aug 26	6.2

Note. [a]Data previously published in van Breugel et al. (1985).
[b]Data consist of two frequencies 50 MHz apart each with 50 MHz bandwidth. Central frequency is given.

The wide band VLA data were flagged, calibrated, and imaged using the Common Astronomy Software Applications package CASA. The data were first Hanning smoothed to isolate the RFI interference peaks and remove Gibbs ringing. The data were then flagged for RFI using the standard automated flagging procedures *TFCrop* and *RFlag* in CASA.

To calibrate the instrumental polarization and correct for the polarization angle, a polarized model for 3C 286 was used, as polarization angle and fractional polarization are known for this source. This was done (using *setjy* and *polcal* in CASA) because due to scheduling issues the parallactic angle coverage for these observations was not sufficient to solve for the calibrator polarization independently. Due to an unresolved issue with the polarization leakage calibration, only two thirds of the scans of Coma A for the 2–4 GHz data had stable amplitudes and phases for polarized correlations. This was indicated by noisy and irregular values in the corrected amplitudes and phases of the scans for 3C 286 adjacent to scans of Coma A. The 2–4 GHz data that did not display stable polarized amplitudes and phases were not used in the analysis.

The data were self-calibrated over the full spectral range for each data set using a multiterm multifrequency synthesis method for imaging. This was done to reduce the noise level in the image, and the wide-band image provided the most accurate model for self-calibration.

For the model fitting, data cubes of Q and U images were made by imaging the data in discreet frequency bins of 8 MHz. A Clark clean was used for each separate Stokes parameter. The visibility data were tapered in the imaging process and the resulting images smoothed all to the same beam size of 7 arcsec, which corresponded to the 1 GHz image. This resulted in data cubes with 126 images along the spectral axis from 1 to 2 GHz.

For the 2–4 GHz data, the instrumental polarization calibration was not ideal; the quality of the per-channel instrumental polarization calibration was poor, due to the small range of parallactic angle coverage for the polarization leakage calibrator source. As a result significantly larger frequency bins were used in the imaging process. This was done in an attempt to reduce the effects of the Stokes Q and U values varying over each spectral window. The visibility data were tapered and images smoothed so that all resulting images had an identical 4.1 arcsec circular beam

Cubes of Stokes Q and U images were made with frequency bins of 128 MHz from 2 to 4 GHz. The resulting cubes have 16 evenly spaced images along the frequency axis.

2.2 Archival VLA observations

To examine the behaviour at higher frequencies, and confirm the observed polarization structure at lower frequencies archival observations at 4.9 and 15 GHz were used. The archival data are also at a higher resolution than the more recent wide-band observations. The raw data were downloaded from the VLA archive and calibrated again for this publication. These observations were useful in localizing exact regions where depolarization occurs. A summary of the archival data analysed is given in Table 2, where ν is the observing frequency. The width of each channel in the wideband setup is $\Delta\nu$. The date is the observing date while t is the total integration time on Coma A for that observation.

In addition to confirming the results of the VLA observations, the archival VLA data were used to investigate the polarization behaviour at higher frequencies and resolutions, where higher fractional polarization was expected. These were calibrated using the Astronomical Image Processing System (AIPS) software package and the resulting visibility data were exported to CASA for imaging using a multiscale CLEAN. Images of the polarized intensity were made with the standard polarization bias correction applied in CASA (e.g. VLA memo 161; Leahy & Fernini 1989). The fractional polarization images were made using only Stokes I as a blanking factor, in this case a blanking limit of 1 mJy beam^{-1} in Stokes I was used. This was important for mapping the heavily depolarized regions that are present even at high frequencies (4.9 and 15 GHz).

2.3 Hα observations

The deep Hα image used in this paper is taken from Tadhunter et al. (2000), which was observed with the William Herschel Telescope in 1998 January. The image is the result of a deep 2 × 900 second integration and has been continuum subtracted to show the pure Hα emission. Further details about the observations and the calibration of this data can be found in Tadhunter et al. (2000).

3 QU MODEL FITTING PROCEDURE

To analyse the polarization and Faraday rotation properties of the lobes of Coma A, we fit the data with an external Faraday dispersion model, as described in Section 1.2. However, to initially identify regions with significant polarization the cubes of Stokes Q and U images were first processed using RM synthesis (Brentjens & de Bruyn 2005). This was done using the PYTHON implementation of *pyrmsynth*.[1] The resulting total polarized flux image from the RM synthesis procedure was used to make a mask for the Q and U cubes. Only regions where the polarized flux in this image was greater than three times the noise level were included in the Q and U cubes. This was done as initial inspections of model fits showed that frequency dependant instrumental polarization was contaminating the data in regions of low signal to noise. It must also be noted that due to this instrumental polarization effect, the 1–2 and 2–4 GHz data sets were analysed and modelled independently.

Before the model fitting, the Q and U cubes were converted to fractional Q and U cubes (referred to as q and u). This was done using model Stokes I images constructed from a spectral index map,

[1]http://mrbell.github.com/pyrmsynth

Downloaded from https://academic.oup.com/mnras/article-abstract/482/4/4606/5173058 by University College Cork user on 21 May 2019

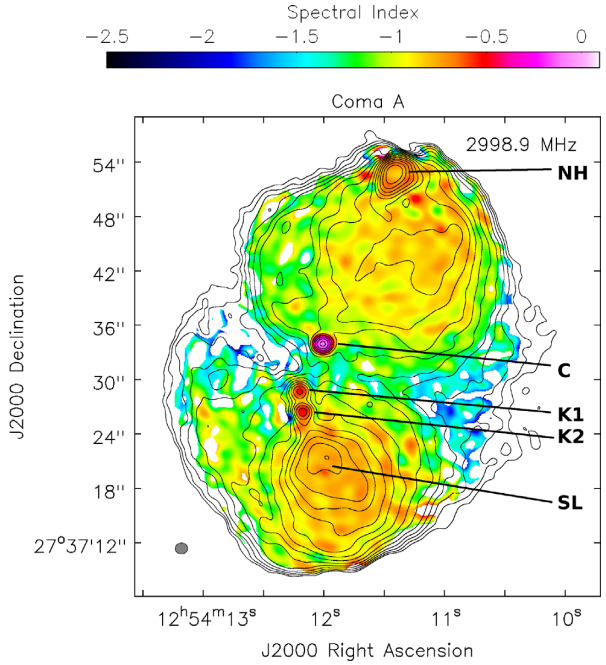


Figure 1. The 2–4 GHz data imaged using a multifrequency synthesis method with a reference frequency at 3 GHz in order to observe the most structure with the best possible resolution. The contours are overlaid on the spectral index map used in the imaging process. The convolving beam is 1.37 × 1.23 arcsec at a position angle of –88.6°. The labelled features are: The northern hotspot (**NH**), core (**C**), knots (**K1** and **K2**), and the southern lobe (**SL**). The contours in Stokes *I* are 0.2 mJy beam^{-1} × (1, 1.41, 2, 2.83, 4, 5.66, 8, 11.31, 16, 22.63, 32, 45.25, 64).

which was made from the multifrequency synthesis imaging, and an image at the central frequency for that band. This was done to avoid regions with negative Stokes *I* arising from dynamic range issues due to the brightness of Coma A and the narrow bands used in making the cubes. This also limited the propagation of noise fluctuations in the Stokes *I* images to the *q* and *u* data.

The cubes were fit according to the model in equations (7a) and (7b). A single component RM model was used with a depolarization term from an external screen, which is what was expected from the Hα measurements and previous publications indicating a gas shell surrounding the lobes. The fitting was done for every unmasked pixel in the cubes using an 'asexual genetic algorithm' (Cantó, Curiel & Martínez-Gómez 2009), which is very efficient in converging to the global best fit. The best-fitting model values were quantified by minimizing the chi-squared function for each fit in each pixel. The results of this fitting were values of χ_0, RM, $\sigma_{\rm RM}$, and p_0 for each unmasked pixel. The pixels from the resulting maps were also blanked according to the error in the model fit. For this the error in the $\sigma_{\rm RM}$ was a good discriminator between acceptable model fits and those contaminated by any remaining residual leakage errors in the low polarization regions.

4 RESULTS

4.1 Radio structure of Coma A

In Fig. 1 we present a Stokes *I* contour map of Coma A overlaid on the spectral index map. This image was made from the 2–4 GHz data and imaged using the multifrequency synthesis method centred on 3 GHz using three Taylor terms in the CASA task *tclean*. The spectral index map, made using only the 2–4 GHz data was cross checked with an interband spectral index map made using the central frequencies from both the 1–2 and 2–4 GHz data (at a lower resolution of 4 arcsec), finding consistent values with the higher resolution 2–4 GHz spectral index map. Additionally the values for spectral index calculated for Coma A in van Breugel et al. (1985) using 1.4 and 4.9 GHz data agree with Fig. 1 also. The northern hotspot, the knots K1 and K2, which were first identified and named in Bridle et al. (1981), and the southern lobe have been labelled. The hotspot to the north is typical for an FRII galaxy showing where the jet is impacting with the IGM. The knot K1 shows the location where the jet is colliding with a gas cloud, which can be identified in optical images (see right-hand panel of figure 8 in Worrall et al. 2016). The K2 knot and diffuse lobe are due to the deceleration of the jet after the deflection of ∼30° from the radio axis on the plane of the sky. The core has a relatively flat spectrum of $\alpha \simeq -0.1$, while outer features all have $\alpha \simeq -0.7$ or less, showing a steeper spectrum typical of optically thin synchrotron emission and older regions of the jet emission.

4.2 QU model fitting

The model fitting showed that a single component RM and external depolarizing random screen provided an excellent fit to the data (Figs 2 and 3). The images of the calculated fitting parameters, RM, $\sigma_{\rm RM}$, p_0, and χ_0 can be seen in Figs 4 and 5.

4.2.1 Northern lobe

The northern hotspot did not have detectable polarization ($\leq$ 0.4 per cent) in the 1–2 GHz range making the model fits poor. This is most likely due to depolarization from large RM variations in addition to intrinsic differences in polarization angle within the 7 arcsec beam across the complex hotspot structure. The fractional polarization for the hotspot was also low in the 2–4 GHz observation where only some polarization is seen to the immediate east and west of the hotspot (ranging from ∼2 per cent to 4 per cent). The centre of the hotspot has been blanked due to high error in the fits and low polarization. To confirm this, the archival data set at 4.9 GHz (Fig. 7a) was used as a reference. The polarized intensity at the exact hotspot is too faint to detect (1 per cent), only to the North and South of the hotspot is polarization reliably measured with values ranging between 2 per cent and 9 per cent, this confirms the results for the wideband 2–4 GHz observations. The 15 GHz observations at a similar resolution show some polarization (Fig. 7d) for the hotspot at around 15 per cent; however, this frequency corresponds to a λ^2 value of 4×10^{-4} m^2 which is close to zero wavelength. This indicates there is strong depolarization in the hotspot region. Note also that the lower 4 arcsec resolution used in the wide band 2–4 GHz observations may also lead to additional depolarization.

The Northern lobe as a whole shows a patchy polarization distribution, presumably due to Faraday depolarization from the Hα emitting gas, as the polarized emission is strongly anticorrelated with the Hα emission (Figs 7b and d). The RM distribution is shown in the histogram in the top panel of Fig. 6 with a mean (median) RM of 34.9 (24.9) rad m^{-2} and standard deviation (median absolute deviation) of 39 (22.6) rad m^{-2}. The high depolarization in the northern hotspot and lobe as a whole can be interpreted as an example of the Laing–Garrington effect (Garrington et al. 1988; Laing 1988), which implies that the northern jet is receding

Downloaded from https://academic.oup.com/mnras/article-abstract/482/4/4606/5173058 by University College Cork user on 21 May 2019

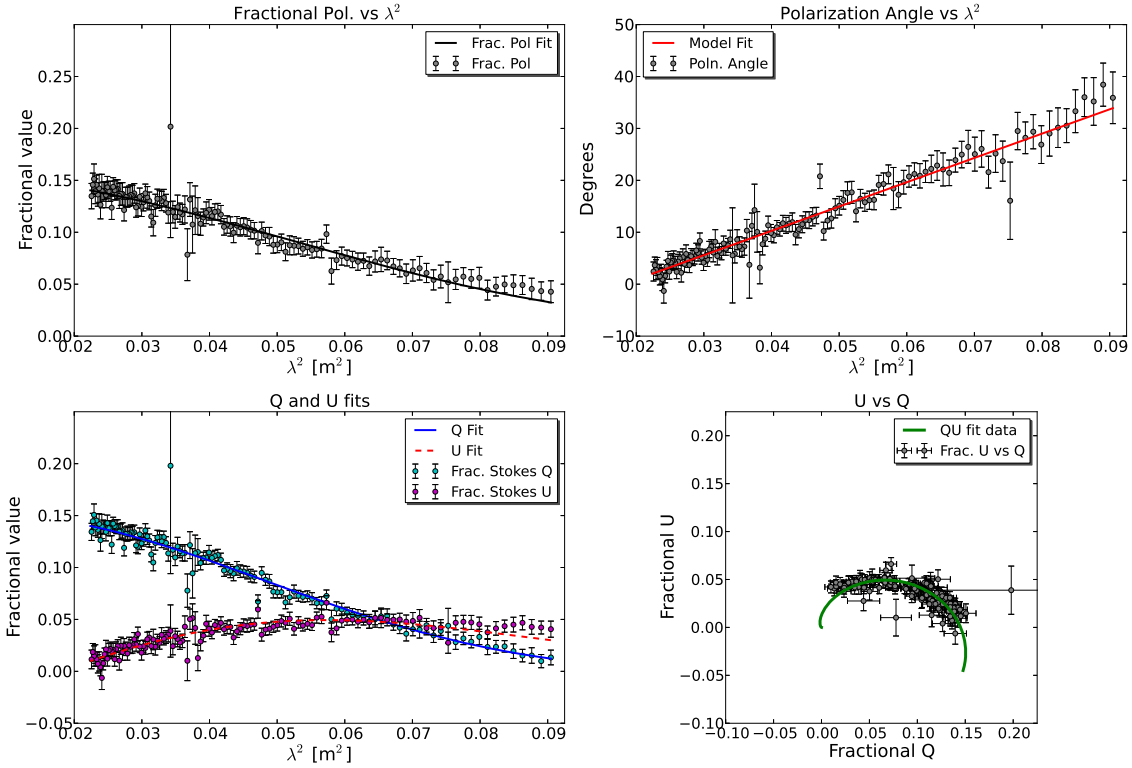


Figure 2. Model fit for the 1–2 GHz data. This is in the upper north western region of the southern lobe, where the polarized flux is the highest. The bottom left panel shows the individual fractional Stokes Q and U fits. The upper left panel shows how the fractional polarization changes with wavelength squared (λ^2). This is made using $p = \sqrt{q^2 + u^2}$ from the fit data in the panel below it. Similarly for the top right panel the actual polarization angle data is plotted. The line passing through is calculated from the fit data as $\chi = 0.5 \arctan(u/q)$, not a linear fit. The bottom right panel simply plots the fractional Stokes Q and U against each other with model fitted data overlaid, the fitted line has been extended in λ^2 to show the fit spiralling towards the origin due to the depolarization. From this fitted region the fit values are: $p_0 = 0.15 \pm 0.001$, RM $= 3.9 \pm 0.1$ rad m^{-2}, $\sigma_{\rm RM} = 9.8 \pm 0.1$ rad m^{-2}, $\chi_0 = -8.5 \pm 0.2^\circ$.

relative to the observer and the southern, more strongly polarized jet is approaching. The fat projected shape of the lobes is also consistent with an orientation significantly inclined to the plane of the sky. One caveat to this is that the southern jet, having been deflected by the collision in K1, has altered its orientation significantly relative to the inner radio axis.

4.2.2 *Southern lobe*

The polarization data for the southern lobe agrees very well with the model in the 1–2 GHz range, as can be seen, for example, in Fig. 2 (The data corresponds to the location indicated by the asterisk in Fig. 4). At this pixel location, $p_0 = 0.15 \pm 0.001$, RM $= 3.9 \pm 0.1$ rad m^{-2}, $\sigma_{\rm RM} = 9.8 \pm 0.1$ rad m^{-2}, and $\chi_0 = -8.5 \pm 0.2^\circ$. The model fit parameters from the 2–4 GHz data, at the same location, are $p_0 = 0.33 \pm 0.03$, RM $= 12 \pm 4$ rad m^{-2}, $\sigma_{\rm RM} = 25.6 \pm 6$ rad m^{-2}, and $\chi_0 = -14 \pm 3^\circ$. This shows the value of the higher resolution data at 2–4 GHz (4 arcsec beam size) which more robustly probes the underlying Faraday rotation variations across the lobes. In particular, the higher value of p_0 indicates that we have resolved most of the RM structure in this region, as the fractional polarization at 15 GHz in this region is ∼0.35 (Fig. 7c). Considering that the model of a Faraday depolarizing screen fits well to the data, the difference in the RM and $\sigma_{\rm RM}$values between 1–2 GHz and 2–4 GHz can be ascribed to resolution dependent effects for an inhomogeneous Faraday screen produced by the patchy distribution of Hα across the lobes.

Looking at the fractional polarization images for the higher resolution archival observations at 4.9 and 15 GHz, there are two regions of appreciably low fractional polarization. First there is a region of low polarization along the centre of the jet in the region after the knot K2. The fractional polarization at 15 GHz varies from ∼14 per cent in the centre to over 30 per cent on either side of this region. This may be due to entrainment of external medium into the jet after deceleration following the collision with K1 (van Breugel et al. 1985) or wavelength-independent depolarization due to the jet magnetic field orientation being roughly orthogonal to the magnetic field orientation in the surrounding lobe. However a toroidal or helical field in the jet giving high fractional polarization at the edges may be another explanation for this feature, which is discussed in Knuettel, Gabuzda & O'Sullivan (2017).

The second feature is a 'trough' in polarized flux in a band transverse to the southern lobe, visible in both the 4.9 and 15 GHz fractional polarization images (Figs 7a and c). At 15 GHz, the fractional polarization in the 'trough' is estimated to be ≤ 3 per cent. What is interesting about this feature is how the lack of polarized emission in this 'trough' correlates with a large filament of Hα emission. Figs 7(b) and (d) and show images of the polarized flux and Hα emission for both frequencies. This indicates that a random magnetic field component coupled with a high electron density within a beamwidth in this 'trough' is causing very significant depolarization, even at 15 GHz. An estimate of the magnetic field and depolarization in this region is made in Section 4.3.

The maps of the various parameters from the model fitting in Figs 4 and 5 do not have a high enough resolution to show the

Downloaded from https://academic.oup.com/mnras/article-abstract/482/4/4606/5173058 by University College Cork user on 21 May 2019

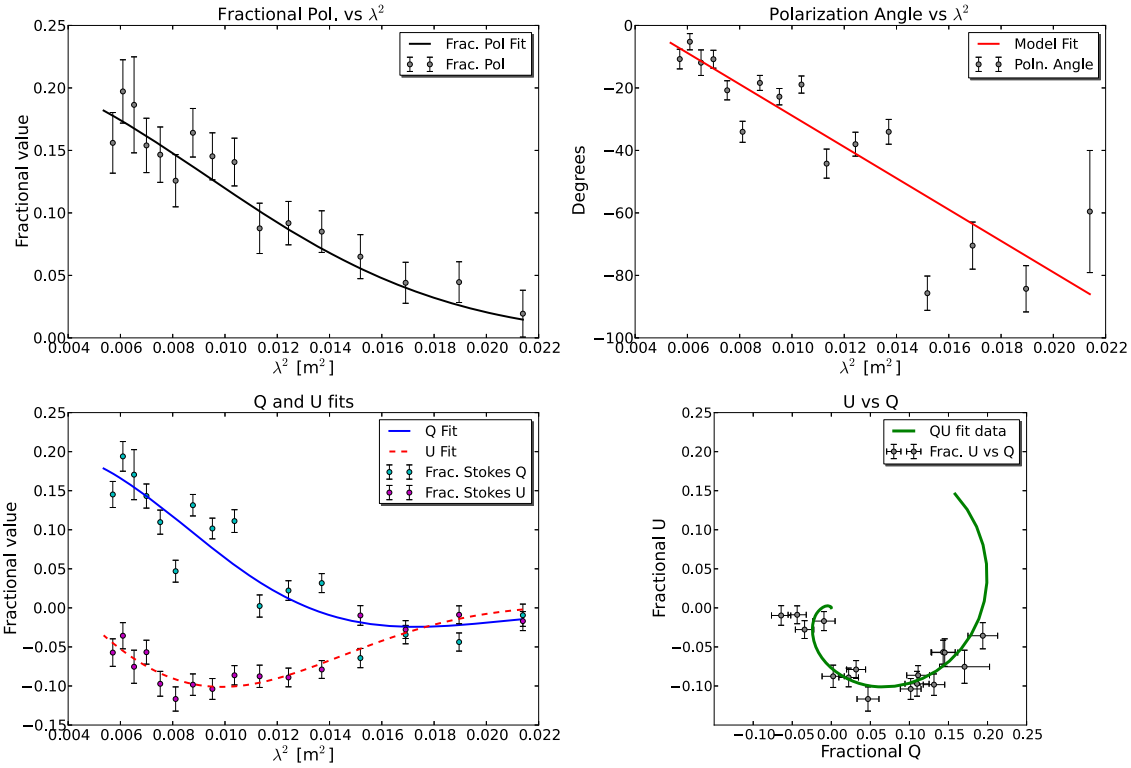


Figure 3. Model fit data for the 2–4 GHz data. This is for a region just to the south west of the Hα filament in the southern lobe. Note the strong depolarization. The graphs panels are displayed in an identical manner as in Fig. 2. From this fitted region the fit values are: $p_0 = 0.22 \pm 0.03$, RM $= -88 \pm 7$ rad m^{-2}, $\sigma_{\rm RM} = 54 \pm 7$ rad m^{-2}, $\chi_0 = -69 \pm 4^\circ$.

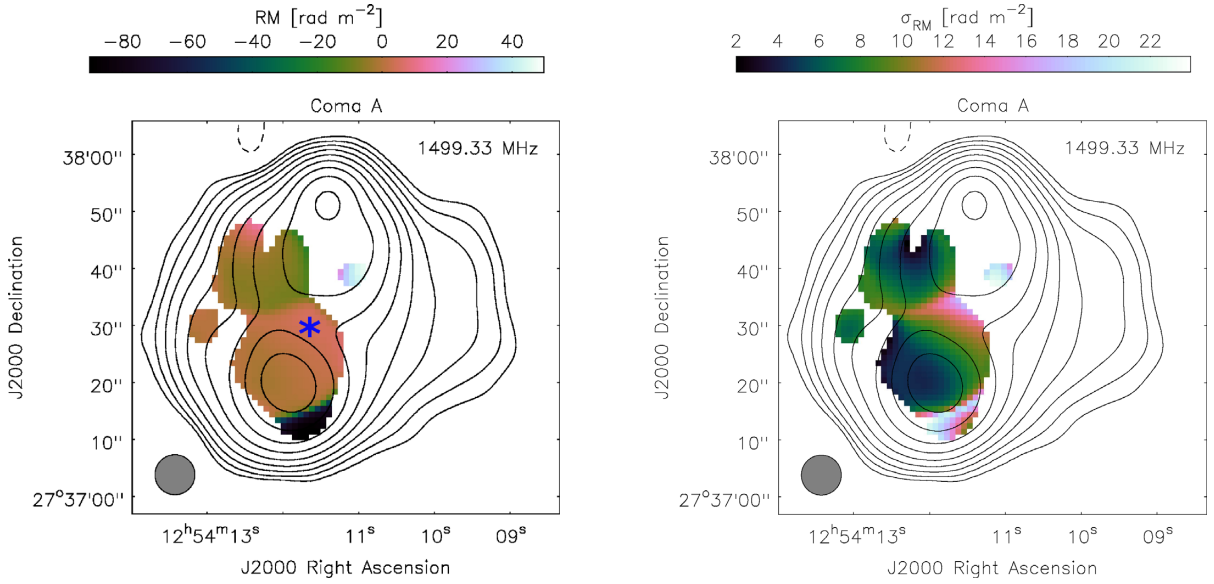


Figure 4. These are the RM (left) and $\sigma_{\rm RM}$ (right) images produced from the model fitting of the 1–2 GHz data. Due to the low resolution used, images of the fractional polarization at zero wavelength (p_0) and intrinsic polarization angle (χ_0) are not included. Note that the blue '$*$' is the location for which the data in Fig. 2 are plotted. For the Stokes *I* contours, a 1–2 GHz image made using a multifrequency synthesis technique is used. The UV data were tapered and the image smoothed to the same 7 arcsec resolution as the images used in the model fit. The central frequency is given in the top right corner of the images. The contours are given at the levels of 1 mJy beam^{-1} × (1, 2, 4, 8, 16, 32, 64, 128, 256).

'trough', however, the parameters change drastically downstream in the jet after this feature. This can be seen in the histogram plots of the RMs for these regions (see bottom panel of Fig. 6). Upstream from the filament the mean (median) RM is 8.4 (7.7) rad m^{-2} with standard deviation (median absolute deviation from the median) of 10 (4.9) rad m^{-2}, whereas after the filament, the RM has a mean (median) value of -83.3 (-90.3) rad m^{-2} and much higher standard deviation (median absolute deviation) of 75.4 (40.3) rad m^{-2}.

Downloaded from https://academic.oup.com/mnras/article-abstract/482/4/4606/5173058 by University College Cork user on 21 May 2019

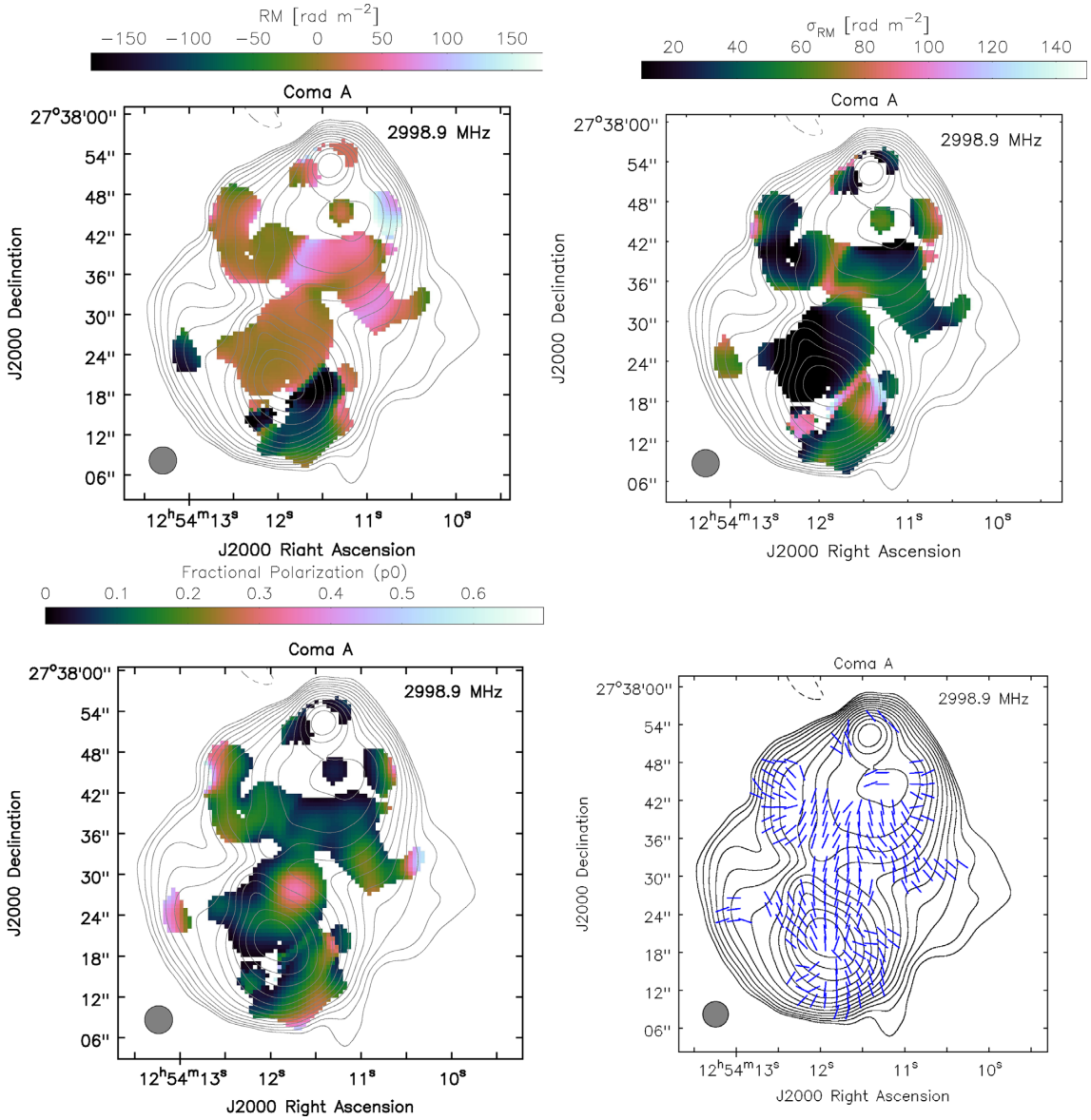


Figure 5. These are the RM (top left) and σ_{RM} (top right) images produced from the model fitting procedure for the 2–4 GHz data. The images of the fractional polarization at zero wavelength (p_0) and intrinsic polarization angle (χ_0) are given on the bottom left and bottom right, respectively. The images were blanked according to the errors in σ_{RM} as this parameter had the highest errors and was a good indicator of the general quality of a fit for a depolarization model. The Stokes *I* contours are from a 2–4 GHz image made using a multifrequency synthesis method using a central frequency of 3 GHz. The image was tapered and smoothed to the same 4.1 arcsec resolution as images used in model fit. The contours are given at the levels 1.4 mJy beam^{-1} × (−1, 1, 1.41, 2, 2.83, 4, 5.66, 8, 11.31, 16, 22.63, 32, 45.25, 64) with the negative contour dashed.

The region after this filament also has a larger amount of Faraday depolarization, as can be seen from the data and model fit in Fig. 3. The large depolarization of $\sigma_{RM} = 54 \pm 7 \mathrm{rad\,m^{-2}}$, is typical for this region and can explain why only a small part of this region is detected in the 1–2 GHz data (Fig. 4). The systematically higher values of σ_{RM} after the filament can also be seen in the map of σ_{RM} values in Fig. 5.

This drastic change in the RM downstream from the jet in the southern lobe is an indicator that the jet/lobe has undergone a significant change in morphology or has interacted with external media. The presence of the Hα filament suggests the latter, especially as this behaviour is not mirrored in the northern lobe. The evidence provided by Morganti et al. (2002) that the lobe is expanding into a disc of neutral gas and ionizing it, creating the filaments observed, is a viable explanation for the depolarizing 'trough' feature. However, a potential complication to any models where there is a giant gas disc perpendicular to the radio jet axis (e.g. Gopal-Krishna & Wiita 2000b), is the likely large inclination of the radio jet axis with respect to the line of sight (as evidenced by the fat-double shape of the lobes, and the Laing–Garrington effect). This would imply that any Hα filament related to this disc material is most likely behind the southern lobe, unless the southern jet has a large deflection back into some of this disc material. Further observations of the complex gas dynamics in this system are warranted.

Downloaded from https://academic.oup.com/mnras/article-abstract/482/4/4606/5173058 by University College Cork user on 21 May 2019

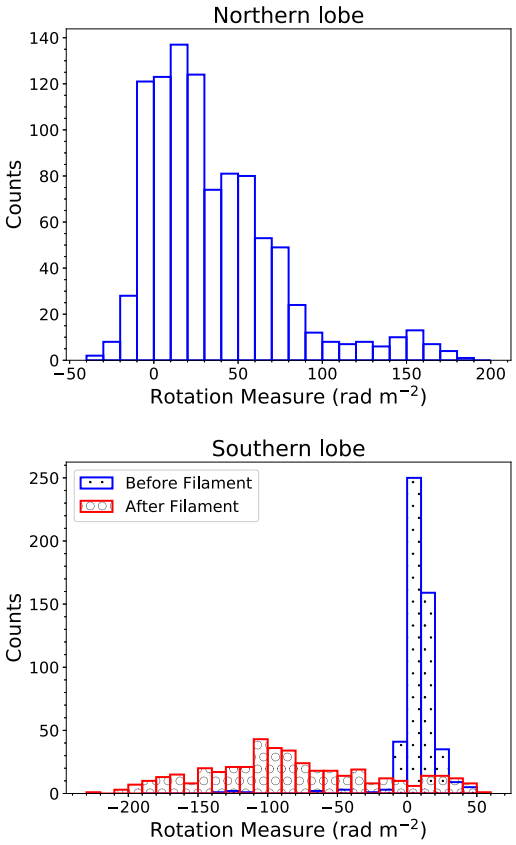


Figure 6. Histograms of the RM distribution in the lobes of Coma A taken from the RM image made for the *S*-Band model fit results. The top panel is the histogram of the RM distribution across the Northern lobe. The bottom panel shows the RM distribution in the Southern lobe, the blue histogram represents the part of the jet before the depolarizing Hα filament and the red histogram represents the RM values after the filament and including the RM feature to the east.

4.3 Estimation of magnetic field strengths

The depolarization by the Hα gas makes it challenging to detect the polarized emission. However, in some regions where there are reliable RM, $\sigma_{\rm RM}$, and Hα values, an estimate of the magnetic field strength within the ionized gas shell can be made. The strong anti-correlation between the Hα emission and the polarization (Fig. 7) is highly indicative that the Faraday rotation (and depolarization) is mainly occurring in the Hα emitting shell around Coma A, as opposed to the extended hot X-ray emitting gas that is also likely present (Worrall et al. 2016). Therefore, this makes a combination of an estimate of the electron density from the Hα data, and the Faraday rotation information from the radio data a powerful tool in directly calculating the magnetic field strengths in this region. Here we follow the method outlined by McClure-Griffiths et al. (2010). The electron density is related to the Hα emission through the emission measure, EM:

$$\mathrm{EM} = 2.75\left(T/10^4\,\mathrm{K}\right)^{0.9} I_{\mathrm{H}\alpha} = n_{\rm e}^2 f L, \tag{8}$$

where T is the temperature of the gaseous region in Kelvin, $I_{\mathrm{H}\alpha}$ is the Hα intensity in Rayleigh's (1 Rayleigh $= 5.7 \times 10^{-18}$ erg cm^{-2} s^{-1} arcsec^{-2} at Hα), $n_{\rm e}$ is the electron number density in cm^{-3}, f is a filling factor between 0 and 1, and L is the line of sight depth of the gaseous region in parsecs. Now using the Faraday rotation measure (equation 5) and solving for the average values:

$$\left\langle B_{\parallel}\right\rangle = 1.235\frac{\langle \mathrm{RM}\rangle}{\int n_{\rm e}(l)\,\mathrm{d}l}. \tag{9}$$

It is reasonable to assume the main source of free electrons in the region between the source and observer is the Hα region of thickness L. Expressing the column density of particles in this region along the line of sight as $n_{\rm e} f L = \sqrt{\mathrm{EM} f L} = \int n_{\rm e}(l)\,\mathrm{d}l$, now we can rewrite equation (9):

$$\left\langle B_{\parallel}\right\rangle = 1.235\frac{\langle \mathrm{RM}\rangle}{n_{\rm e} f L}. \tag{10}$$

This gives an estimate of the average line of sight magnetic field in the ionized shell surrounding the radio lobes.

The $\sigma_{\rm RM}$ parameter from Section 1.2 can be used to estimate the strength of the turbulent magnetic field component in the depolarizing shell of ionized gas. This can be calculated by considering the ionized gas as a collection of cells, each with their own Faraday depth and coherent magnetic field, which when combined along the line of sight gives a turbulent depolarizing screen. Using the definition of $\sigma_{\rm RM}$ given in Burn (1966), the diameter of such a cell, d can be estimated as has been done in van Breugel, Heckman & Miley (1984):

$$\sigma_{\rm RM} = 0.81 n_{\rm e}\langle B_{\rm rand}\rangle\sqrt{\mathrm{d}L}. \tag{11}$$

In equation (11) all values except $B_{\rm rand}$ and d can be estimated directly from the data. A range of values for the turbulent cell size can be estimated for each region using reasonable upper limits for $B_{\rm rand}$ and d. The lower limit for the cell size occurs when the value for the magnetic field strength is at maximum within each cell; a reasonable estimate for the maximum magnetic field is the equipartition field strength of the radio lobe in that region. This assumes the Hα gas is completely mixed with the outer region of the lobe and depolarizes the signal, as well as disordering the direction of any magnetic field in the lobe in that region, but maintaining the same field strength in each of the cells of diameter d. The upper limit for d can be taken to be half of the observing beam for the highest resolution observation of Coma A that shows depolarization. van Breugel et al. (1985) have estimated the upper limit for d using this method to be 300 pc for all regions in Coma A, which yields the smallest possible $B_{\rm rand}$ for the given depolarization.

For all our magnetic field calculations in Coma A we assumed $f = 1$, $T = 1 \times 10^4$ K, and $L = 3.5$ kpc. The value used for f assumes full ionization in the gas. The temperature used here has been estimated in van Breugel et al. (1985). The thickness of the shell, L, was calculated by measuring the thickness of the projected shell in the Hα image as seen in the filament of Hα gas in the north-east of the northern lobe (Fig. 7b). It must also be noted that the small Galactic contribution to the RM of 2.3 ± 1.3 rad m^{-2} (Taylor, Stil & Sunstrum 2009) can be safely ignored due to the location of Coma A being very close to the Galactic pole.

4.3.1 Magnetic field strength in Faraday screen of northern lobe

The northern hotspot region shows bright Hα emission and some of the 2–4 GHz polarization data for that region, particularly in the north western region of the hotspot is reliable for fitting (see Fig. 5). Values of RM $\simeq 30$ rad m^{-2}, $\sigma_{\rm RM} \simeq 30$ rad m^{-2}, and $I_{\mathrm{H}\alpha} = 1.4 \times 10^{-16}$ erg cm^{-2}s^{-1} arcsec^{-2} $\equiv 24.6$ Rayleigh were used to estimate the magnetic field in the gas. The calculation also gives an estimate of $n_{\rm e} = 0.13$ cm^{-3} for the electron density, as complete ionization is assumed. This led to a value of $\left\langle B_{\parallel}\right\rangle = 0.07$ μG for the ordered

Downloaded from https://academic.oup.com/mnras/article-abstract/482/4/4606/5173058 by University College Cork user on 21 May 2019

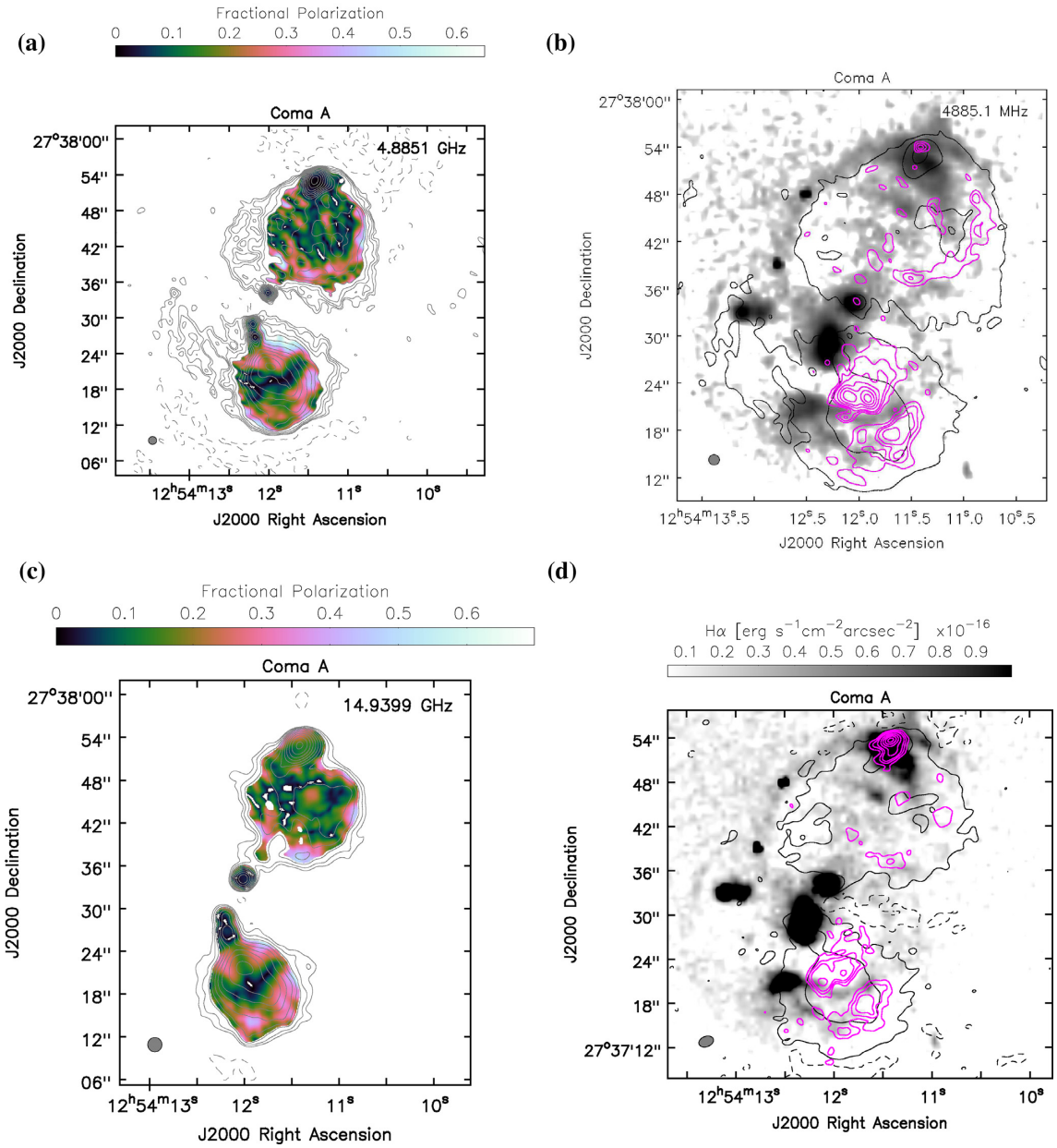


Figure 7. (a) 1.4 arcsec resolution 4.9 GHz image of Coma A from the VLA archival data. The colour image is the debiased fractional polarization where the corresponding Stokes *I* intensity is greater than 1 mJy beam^{-1} at 4.9 GHz and the contours are the total Stokes *I* emission at that same frequency. The contours are given at the levels of 0.25 mJy beam^{-1} × (−1, 1, 1.41, 2, 2.83, 4, 5.66, 8, 11.31, 16, 22.63, 32, 45.25, 64, 90.51) with the negative contour dashed. (b) Image of Coma A showing polarized flux density in Jy beam^{-1} as purple contours with levels at 0.45 mJy beam^{-1} × (1, 1.5, 2, 3, 4, 5, 6). Stokes *I* contours are given in black at 27.5 mJy beam^{-1} × (0.008, 0.2, 0.6) which corresponds to 0.8, 20, and 60 per cent of the peak value. The deep Hα image is given in greyscale. (c) 2 arcsec resolution 15 GHz image of Coma A from the VLA archival data. The colour image is the debiased fractional polarization at 15 GHz displaying only values where the corresponding Stokes *I* value is greater than 1 mJy beam^{-1}. The contours are the total Stokes *I* emission at that same frequency. The contours are given at the levels of 0.45 mJy beam^{-1} × (−1, 1, 1.41, 2, 2.83, 4, 5.66, 8, 11.31, 16, 22.63, 32) with the negative contour dashed. (d) Image of Coma A showing polarized flux density at 15 GHz in Jy beam^{-1} as purple contours with levels at 0.4 mJy beam^{-1} × (1, 1.5, 2, 3, 4, 5, 6, 7). Stokes *I* contours at the same frequency are given in black at 0.2 mJy beam^{-1} × (−1, 1, 8, 32) with the negative contour dashed. The deep Hα image is given in greyscale.

magnetic field in the ionized shell. The random component can be estimated to be $B_{\rm rand} \geq 0.27\,\mu$G using the lower limit to the depolarizing cell size of $d \leq 300$ pc. The smallest possible value for the cell size d is estimated to be $d \simeq 0.008$ pc when the maximum possible magnetic field is assumed to be the equipartition estimate of 54 μG (table 4 in van Breugel et al. 1985) for that region.

The archival data can also be useful for estimating RM and $\sigma_{\rm RM}$, as the higher polarization fraction and range in λ^2 can give better estimates for the magnetic field strengths. Using the high frequency end of the 2–4 GHz data and the 4.9 and 15 GHz archival data sets, a simple linear fit of the polarization angles was used to estimate the RM. To estimate $\sigma_{\rm RM}$, the fractional polarization for the same hotspot region averaged over a 2 arcsec beam size was fit with the exponential part of the depolarization model (equation 6), namely:

$$p(\lambda) = p_0 e^{-2\sigma_{\rm RM}^2 \lambda^4}. \quad (12)$$

Downloaded from https://academic.oup.com/mnras/article-abstract/482/4/4606/5173058 by University College Cork user on 21 May 2019

This method gave RM $\simeq 180\,\mathrm{rad\,m^{-2}}$ and $\sigma_{\mathrm{RM}} \simeq 176\,\mathrm{rad\,m^{-2}}$, which are significantly higher but may better describe the hotspot environment due to the improved resolution.

Using the rotation measure values and the same value for $I_{\mathrm{H}\alpha}$, the magnetic field strengths were calculated to be: $\langle B_{\parallel} \rangle = 0.45\,\mu\mathrm{G}$ and $\langle B_{\mathrm{rand}} \rangle \geq 1.63\,\mu\mathrm{G}$. The smallest possible value for the cell size d is estimated to be $d \simeq 0.5\,\mathrm{pc}$, when, the maximum possible magnetic field is again assumed to be the equipartition estimate of 54 μG for the hotspot. These values are almost an order of magnitude different from the earlier attempt; however, the higher frequency data shows more reliable polarization structure. This estimate is supported by other studies (e.g. Laing et al. 2008; Bonafede et al. 2010; Guidetti et al. 2010) that commonly infer field strengths of 1–10 μG in the hot X-ray emitting gas phase that pervades the ambient intracluster/intragroup medium surrounding radio galaxies. In the case of Coma A, Worrall et al. (2016) argue that faint X-ray emission from thermal gas is also present, indicating a weak group atmosphere.

The random and uniform line-of-sight magnetic field strength estimates of O(1) μG suggest little or no mixing is occurring between the lobe and the surrounding gas near the northern hotspot. However, as the exact size of the depolarizing cell size is unknown, the random magnetic field strength cannot be precisely estimated. In Mao et al. (2008) and Gaensler (2005) a cell size of ∼90 pc is used for the Small and Large Magellanic Clouds. This value falls within the range of values estimated for d and if the conditions in the Coma A Hα region are similar to the ISM in the SMC and LMC the resulting turbulent magnetic field can be estimated as 0.5 μG for the 2–4 GHz results and 3 μG for the results including the archival data at higher frequencies and resolution.

4.3.2 *Magnetic field strength in Faraday screen of southern lobe*

Another interesting region to probe is the depolarizing 'trough' feature transverse to the southern lobe discussed in Section 4.1. It is difficult to estimate RM and σ_{RM} in this region as even at 15 GHz this region has no significant polarization. As the RM changes significantly in the jet downstream from this 'trough', this Hα filament may be causing this. Using a typical RM value for the downstream region, RM $\simeq -80\,\mathrm{rad\,m^{-2}}$, the H$\alpha$ electron number density, $n_{\mathrm{e}} \simeq 0.09\,\mathrm{cm^{-3}}$, and a shell depth of 3.5 kpc, an estimate for the line-of-sight, coherent, magnetic field was calculated to be: $\langle B_{\parallel} \rangle = 0.31\,\mu\mathrm{G}$.

Using the 15 GHz archival data, an estimate of σ_{RM} can be made from the turbulent depolarization model. Assuming that the fractional polarization in regions upstream and downstream from the 'trough' are very close to the intrinsic value at 15 GHz, this implies that $p_{15\,\mathrm{GHz}} \simeq p_0 \simeq 0.3$ for these regions. This is a safe assumption as the model fitting has shown that σ_{RM} is very low in the inner lobe compared to the 'trough' region. We also suppose that the 'trough' region should have the same intrinsic polarization at zero wavelength as the regions on either side if not for strong depolarization by the Hα gas. The fractional polarization in the 'trough' region at 15 GHz can be estimated to be less than 3 per cent polarized ($p(\lambda) \lesssim 0.03$).

Using equation (12) with these assumptions, the resulting σ_{RM} value is $\sigma_{\mathrm{RM}} \geq 2700\,\mathrm{rad\,m^{-2}}$. This results in a random magnetic field strength of $B_{\mathrm{rand}} \geq 36\,\mu\mathrm{G}$ when using the upper limit for the depolarizing cell size of 300 pc to give the lowest limit for this random magnetic field. This is comparable to the equipartition magnetic field strength across the southern lobe of 30–50 μG (van Breugel et al. 1985), and indicates that the Hα gas has mixed with the synchrotron plasma of the lobes. Such strong evidence for internal Faraday rotation depolarization is rare but has been claimed in other recent studies (O'Sullivan et al. 2013; Stawarz et al. 2013; Anderson et al. 2018). There remains a possibility that the pre-existing magnetic field of O(1) μG (as estimated for the Hα gas covering the northern lobe) is amplified significantly by a strong MHD shock, somewhat similar to that expected in supernova remnants (e.g. Schure et al. 2012). However, it seems somewhat inconsistent that the necessary field amplification, by a factor of 30 or more, would occur only near the trough region, and not from the bow shock of the northern lobe also.

In general, there are several potential reasons for the high depolarization. It may be due to a complex interaction between the lobe and the Hα filament, where mixing between the filament and the lobe has occurred or the shock-ionization of the filament mixed with the lobe has compressed it to result in such a high magnetic field strength. Furthermore this filament is spatially correlated with a decrease in the total intensity which can be seen in the contours in Figs 1 and 7(a), and in van Breugel et al. (1985); Fig. 5. It is difficult to explain what is causing this decrease as a dense obstacle should ordinarily compress and enhance the synchrotron emission. However, one possibility given by van Breugel et al. (1985) is that the interaction significantly increases the relative amount of the line-of-sight magnetic field component with respect to the perpendicular component at this location in the lobe. This would have the dual effect of decreasing the observed synchrotron emission and increasing internal Faraday rotation (and depolarization) at this location. This appears plausible as the magnitude of the RM is at its highest downstream of the filament, indicating a stronger line-of-sight magnetic field component and the depolarization is very high in the filament region with $\sigma_{\mathrm{RM}} \geq 2700\,\mathrm{rad\,m^{-2}}$.

Another possibility is that there is mass entrainment in the jet, shown by the region of low polarization along the jet centre in the southern lobe, and material has been 'dumped' in the transverse 'trough' region, which was proposed by van Breugel et al. (1985). This however is not an explanation for the high levels of Hα emission in the 'trough'/filament as no such emission is seen along the centre of the jet. The Hα filaments also extend along the entire eastern side of Coma A including the northern lobe, where there is no evidence of mass entrainment. Therefore, we find that the most plausible scenario is that the Hα gas shell is close to but external to the radio lobes, except in the 'trough' region of the southern lobe, where the Hα gas is mixing with the lobe plasma.

5 CONCLUSIONS

We have presented a comprehensive broad-band radio polarization and Faraday rotation study of the nearby radio galaxy Coma A. Broad-band VLA observations in the 1–2 and 2–4 GHz ranges were analysed using RM synthesis and qu-model fitting. Large variations in the observed degree of polarization were observed over the radio galaxy which is indicative of Faraday depolarization. Large variations in the RM were also observed across the southern lobe, indicating a substantial change in the morphology of the jet and lobe. In conjunction with this, higher resolution archival observations at 4.9 and 15 GHz were also analysed along with deep Hα observations showing strong spatial correlation with the depolarized regions and the Hα emission.

We find that an external Faraday depolarizing screen is consistent with the broad-band polarization data across the majority of the radio lobes. Due to the clear anticorrelation between the polarized

Downloaded from https://academic.oup.com/mnras/article-abstract/482/4/4606/5173058 by University College Cork user on 21 May 2019

emission and Hα, this external Faraday screen is identified as the ionized gas seen in Hα arcs and filaments surrounding the radio lobes. The Hα emission is most likely caused by shock-ionization of a gas disc (seen in neutral hydrogen) by the expanding radio lobes.

We used the Hα image in combination with the Faraday rotation and depolarization results to estimate the magnetic field strength in this ionized gas. We derived magnetic field strengths in the Hα gas of $\sim$1 μG across most of the radio lobes, consistent with expectations for the magnetization of gas in the local IGM. However, one particular Hα filament that cuts across the southern lobe is clearly associated with a strong depolarization 'trough', and has a magnetic field strength similar to the equipartition field strength in the lobes (i.e. $\gtrsim$36 μG). This implies that the Hα gas in this filament has mixed with the radio-emitting plasma of the lobes. This is one of the clearest direct observational examples of internal Faraday depolarization in the lobe of a radio galaxy. This adds to the complex ways that radio jets and lobes can interact with their environment, providing another means of 'feedback' on local gas, that can both inhibit further star formation activity and substantially modify the evolution of radio galaxies.

ACKNOWLEDGEMENTS

This research has been funded by the Irish Research Council under the Government of Ireland Postgraduate Programme. The VLA is an instrument of the National Radio Astronomy Observatory, a facility of the National Science Foundation operated under cooperative agreement by Associated Universities, Inc. The authors would like to thank Clive Tadhunter for the Hα image of Coma A and Denise Gabuzda for useful discussion and feedback during the writing of this manuscript. The authors also wish to thank the referee, Dr. J. P. Leahy, for his thoughtful feedback which improved this paper. SPO acknowledges financial support from the Deutsche Forschungsgemeinschaft (DFG) under grant BR2026/23 and from UNAM through the PAPIIT project IA103416.

REFERENCES

Anderson C. S., Gaensler B. M., Heald G. H., O'Sullivan S. P., Kaczmarek J. F., Feain I. J., 2018, ApJ, 855:41, 27
Bonafede A., Feretti L., Murgia M., Govoni F., Giovannini G., Dallacasa D., Dolag K., Taylor G. B., 2010, A&A, 513, A30
Brentjens M. A., de Bruyn a. G., 2005, A&A, 441, 1217
Bridle A. H., Fomalont E. B., Palimaka J. J., Willis A. G., 1981, ApJ, 248, 499
Burn B. J., 1966, MNRAS, 133, 67
Cantó J., Curiel S., Martínez-Gómez E., 2009, A&A, 501, 1259
Chiaberge M., Capetti A., Celotti A., 1999, A&A, 349, 77
de Gasperin F., 2017, MNRAS, 467, 2234
Fabian A. C., 2012, ARA&A, 50, 455
Fanaroff B. L., Riley J. M., 1974, MNRAS, 167, 31P
Gaensler B. M., 2005, Science, 307, 1610
Garrington S. T., Leahy J. P., Conway R. G., Laingt R. A., 1988, Nature, 331, 147
Gawronski M. P., Marecki A., Kunert-Bajraszewska M., Kus A. J., 2006, A&A, 447, 63
Gopal-Krishna , Wiita P. J., 2000a, A&A, 363, 507
Gopal-Krishna , Wiita P. J., 2000b, ApJ, 529, 189
Guidetti D., Laing R. A., Murgia M., Govoni F., Gregorini L., Parma P., 2010, A&A, 514, 50
Heckman T., Best P., 2014, ARA&A, 52, 589
Knuettel S., Gabuzda D., O'Sullivan S., 2017, Galaxies, 5, 61
Laing R. A., 1988, Nature, 331, 149
Laing R. A., Bridle A. H., Parma P., Murgia M., 2008, MNRAS, 391, 521
Leahy P., Fernini I., 1989, VLA Scientific Memorandum No. 161; Correction Schemes for Polarized Intensity. NRAO Library, National Radio Astronomy Observatory
Mao S. A., Gaensler B. M., Stanimirović S., Haverkorn M., McClure-Griffiths N. M., Staveley-Smith L., Dickey J. M., 2008, ApJ, 688, 1029
McClure-Griffiths N. M., Madsen G. J., Gaensler B. M., McConnell D., Schnitzeler D. H. F. M., 2010, ApJ, 725, 275
Morganti R., Oosterloo T. A., Tinti S., Tadhunter C. N., Wills K. A., van Moorsel G., 2002, A&A, 387, 830
O'Sullivan S. P. et al., 2012, MNRAS, 421, 3300
O'Sullivan S. P. et al., 2013, ApJ, 764, 162
Planck Collaboration et al., 2016, A&A, 594, A11
Schure K. M., Bell A. R., O'C Drury L., Bykov A. M., 2012, Space Sci. Rev., 173, 491
Sokoloff D. D., Bykov A. A., Shukurov A., Berkhuijsen E. M., Beck R., Poezd A. D., 1998, MNRAS, 299, 189
Stawarz et al., 2013, ApJ, 766, 48
Tadhunter C. N., Villar-Martin M., Morganti R., Bland-Hawthorn J., Axon D., 2000, MNRAS, 314, 849
Taylor A. R., Stil J. M., Sunstrum C., 2009, ApJ, 702, 1230
van Breugel W., Heckman T., Miley G., 1984, ApJ, 276, 79
van Breugel W., Miley G., Heckman T., Butcher H., Bridle A., 1985, ApJ, 290, 496
Worrall D. M., Birkinshaw M., Young A. J., 2016, MNRAS, 458, 174
Wright E. L., 2006, PASP, 118, 1711

This paper has been typeset from a TEX/LATEX file prepared by the author.

Downloaded from https://academic.oup.com/mnras/article-abstract/482/4/4606/5173058 by University College Cork user on 21 May 2019